

# Higgs boson production at the LHC using the $q_T$ subtraction formalism at N<sup>3</sup>LO QCD

Leandro Cieri<sup>(a,b)</sup>, Xuan Chen<sup>(b)</sup>, Thomas Gehrmann<sup>(b)</sup>,  
E.W.N. Glover<sup>(c)</sup> and Alexander Huss<sup>(d)</sup>

<sup>(a)</sup> INFN, Sezione di Milano-Bicocca,  
Piazza della Scienza 3, I-20126 Milano, Italy

<sup>(b)</sup> Physik-Institut, Universität Zürich, CH-8057 Zurich, Switzerland

<sup>(c)</sup> Institute for Particle Physics Phenomenology, Durham University, Durham, DH1 3LE, UK

<sup>(d)</sup> Theoretical Physics Department, CERN, 1211 Geneva 23, Switzerland

## Abstract

We consider higher-order QCD corrections to Higgs boson production through gluon-gluon fusion in hadron collisions. We use the transverse-momentum ( $q_T$ ) subtraction method at the next-to-next-to-next-to-leading order (N<sup>3</sup>LO) to numerically compute arbitrary infrared-safe observables for this class of processes. To cancel the infrared divergences, we exploit the universal behaviour of the associated  $q_T$  distributions in the small- $q_T$  region. Our calculation is implemented in a parton level Monte Carlo program that allows the user to apply arbitrary kinematical cuts on the associated jet activity, and to compute the corresponding distributions in the form of bin histograms. We present selected numerical results at the LHC.

# 1 Introduction

## 2 The $q_T$ subtraction formalism at N<sup>3</sup>LO

This section is devoted to the presentation of the transverse-momentum subtraction formalism at N<sup>3</sup>LO in perturbative QCD. The method is illustrated in general form and special attention is paid to the case of Higgs boson production through gluon–gluon fusion. The  $q_T$  subtraction formalism presented in this section is the extension of the subtraction method originally proposed in Refs. [1, 2, 3].

We consider the inclusive hard-scattering reaction

$$h_1(p_1) + h_2(p_2) \rightarrow F(\{q_i\}) + X, \quad (1)$$

where  $h_1$  and  $h_2$  are the two hadrons which collide with momenta  $p_1$  and  $p_2$  producing the triggered final-state system  $F$ , accompanied by an arbitrary and undetected final state  $X$ . The colliding hadrons with centre-of-mass energy  $\sqrt{s}$ , are treated as massless particles ( $s = (p_1 + p_2)^2 = 2p_1p_2$ ). The observed final state  $F$  consist of a generic system of non-QCD partons composed by *one* or *more* colour singlet particles (such as *one* or *more* vector bosons ( $\gamma^*, W, Z, \dots$ ), photons, Higgs particles, Drell–Yan (DY) lepton pairs and so forth) with momenta  $q_i^\mu$  ( $i = 3, 4, 5, \dots$ ). The total momentum of the system  $F$  is denoted by  $q^\mu$  ( $q = \sum_i q_i$ ) and it can be expressed in terms of the total invariant mass  $M$  ( $q^2 = M^2$ ), the transverse momentum  $\mathbf{q}_T$  with respect to the direction of the colliding hadrons, and the rapidity  $y$  ( $2y = \ln(p_2 q / p_1 q)$ ) in the centre-of-mass system of the collision. Since  $F$  is colourless, the LO partonic Born cross section can be either initiated by  $qq'$  annihilation, as in the case of the Drell–Yan process or by gluon–gluon fusion as in the case of the Higgs boson production.

In order to report the principles of the subtraction formalism we first notice that at LO, the transverse momentum  $\mathbf{q}_T = \sum_i \mathbf{q}_{T,i}$  of the final state system  $F$  is identically zero. Therefore, as long  $q_T \neq 0$ , the N <sup>$n$</sup> LO contributions (with  $n = 1, 2, 3$ ) are given by the N <sup>$n-1$</sup> LO contributions to the triggered final state  $F + \text{jet(s)}$ . Consequently, if  $q_T \neq 0$  we have:

$$d\sigma_{\text{N}^n\text{LO}}^F(q_T \neq 0) \equiv d\sigma_{\text{N}^{n-1}\text{LO}}^{F+\text{jets}} \quad \text{with } n = 1, 2, 3. \quad (2)$$

The notation N <sup>$n$</sup> LO stands for: N<sup>0</sup>LO=LO, N<sup>1</sup>LO=NLO, N<sup>2</sup>LO=NNLO and so forth. Equation (2) implies that if  $q_T \neq 0$  the infra-red (IR) divergencies that appear in the computation of  $d\sigma_{\text{N}^n\text{LO}}^F(q_T \neq 0)$  are those already present in  $d\sigma_{\text{N}^{n-1}\text{LO}}^{F+\text{jets}}$ . These IR singularities can be handled and cancelled with the available subtraction methods at the NLO and NNLO. The only remaining singularities at N <sup>$n$</sup> LO are associated with the limit  $q_T \rightarrow 0$  and we treat them with the transverse momentum subtraction method. Since the small- $q_T$  behaviour of the transverse momentum cross section is well known thorough the resummation program [5] of logarithmically-enhanced contributions to transverse-momentum distributions, we exploit this knowledge to construct the necessary counterterms (CT) in order to subtract the remaining singularity and promote to N<sup>3</sup>LO Refs. [1, 2, 3]. The precedent strategy is accomplished combining resummed and fixed-order calculations as detailed in [2].

The sketchy form of the  $q_T$  subtraction method [1] for the N <sup>$n$</sup> LO cross section is

$$d\sigma_{\text{N}^n\text{LO}}^F = \mathcal{H}_{\text{N}^n\text{LO}}^F \otimes d\sigma_{\text{LO}}^F + [d\sigma_{\text{N}^{n-1}\text{LO}}^{F+\text{jets}} - d\sigma_{\text{N}^n\text{LO}}^{F\text{CT}}] \quad \text{with } n = 1, 2, 3, \quad (3)$$

where  $d\sigma_{\text{N}^n\text{LO}}^{F\text{CT}}$  is the contribution of the counterterm to the  $\text{N}^n\text{LO}$  cross section which cancels the divergencies of  $d\sigma_{\text{N}^{n-1}\text{LO}}^{F+\text{jets}}$  in the limit  $q_T \rightarrow 0$ . The  $n$ -order counterterm can be written

$$d\sigma_{\text{N}^n\text{LO}}^{F\text{CT}} = \Sigma_{\text{N}^n\text{LO}}^F(q_T^2/M^2) d^2\mathbf{q}_T \otimes d\sigma_{\text{LO}}^F, \quad (4)$$

where the symbol  $\otimes$  manifests convolutions over momentum fractions and sum over flavour indices of the partons. More precisely, the function  $\Sigma_{\text{N}^n\text{LO}}^F(q_T^2/M^2)$  is the  $n$ -order truncation of the perturbative series in  $\alpha_S$

$$\Sigma_{c\bar{c} \leftarrow a_1 a_2}^F(q_T^2/M^2) = \sum_{n=1}^{\infty} \left(\frac{\alpha_S}{\pi}\right)^n \Sigma_{c\bar{c} \leftarrow a_1 a_2}^{F(n)}(q_T^2/M^2), \quad (5)$$

where the labels  $a_1$  and  $a_2$  stands for the partonic channels of the  $\text{N}^n\text{LO}$  correction to the Born cross section ( $d\sigma_{\text{LO}}^F \equiv d[\sigma_{c\bar{c}}^{F(0)}]$ ). Notice that at LO the only available configuration is  $a_1 = c$  and  $a_2 = \bar{c}$ , where  $c\bar{c}$  is (are) the partonic channel(s) at which the LO cross section is initiated. The function  $\Sigma^F(q_T^2/M^2)$  embodies all the logarithmic terms that are divergent in the limit  $q_T \rightarrow 0$  reproducing the singular behaviour of  $d\sigma^{F+\text{jets}}$  in the small- $q_T$  limit. The counterterm is defined free of terms proportional to  $\delta(q_T^2)$  which are all considered in the perturbative factor  $\mathcal{H}^F$ . The hard coefficient function  $\mathcal{H}_{\text{N}^n\text{LO}}^F$  that encodes all the IR finite terms of the  $n$ -loop contributions, is obtained by the  $\text{N}^n\text{LO}$  truncation of the perturbative function

$$\mathcal{H}_{c\bar{c} \leftarrow a_1 a_2}^F(z; \alpha_S) = \delta_{c a_1} \delta_{\bar{c} a_2} \delta(1-z) + \sum_{n=1}^{\infty} \left(\frac{\alpha_S}{\pi}\right)^n \mathcal{H}_{c\bar{c} \leftarrow a_1 a_2}^{F(n)}(z), \quad (6)$$

where  $z = M^2/s$ . According to the transverse momentum resummation formula (Eq. (10) of Ref. [2]) and using the Fourier transformation between the conjugate variables  $q_T$  and  $b$  ( $b$  is the impact parameter), the perturbative hard function  $\mathcal{H}^F$  and the counterterm are obtained by the fixed order truncation of the following identity

$$\begin{aligned} & (\Sigma_{c\bar{c} \leftarrow a_1 a_2}^F(q_T^2/M^2) + \mathcal{H}_{c\bar{c} \leftarrow a_1 a_2}^F(\alpha_S, M)) \otimes d[\sigma_{c\bar{c}}^{F(0)}] = \frac{M^2}{s} \int_0^\infty db \frac{b}{2} J_0(bq_T) S_c(M, b) \\ & \times \int_{x_1}^1 \frac{dz_1}{z_1} \int_{x_2}^1 \frac{dz_2}{z_2} d[\sigma_{c\bar{c}}^{F(0)}] f_{a_1/h_1}(x_1/z_1, b_0^2/b^2) f_{a_2/h_2}(x_2/z_2, b_0^2/b^2) \otimes [H^F C_1 C_2]_{c\bar{c}; a_1 a_2}, \end{aligned} \quad (7)$$

where  $J_0(bq_T)$  is the 0th-order Bessel function,  $f_{c/h}$  corresponds to the distribution of a parton  $c$  in a hadron  $h$  and  $b_0 = 2e^{-\gamma_E}$  ( $\gamma_E = 0.5772\dots$  is the Euler number). The symbolic factor  $d[\sigma_{c\bar{c}}^{F(0)}]$  for the Born cross section  $\sigma_{c\bar{c}}^{F(0)}$  denotes

$$d[\sigma_{c\bar{c}}^{F(0)}] \equiv \frac{d\sigma_{c\bar{c}}^{F(0)}}{d\phi}, \quad (8)$$

where  $\phi$  represents the phase-space of the final state system  $F$ . The large logarithmic corrections are exponentiated in the Sudakov form factor  $S_c(M, b)$  of the quark ( $c = q, \bar{q}$ ) or of the gluon ( $c = g$ ), and it has the following expression:

$$S_c(M, b) = \exp \left\{ - \int_{b_0^2/b^2}^{M^2} \frac{dq^2}{q^2} \left[ A_c(\alpha_S(q^2)) \ln \frac{M^2}{q^2} + B_c(\alpha_S(q^2)) \right] \right\}. \quad (9)$$

The functions  $A$  and  $B$  in Eq. (9) are perturbative series in  $\alpha_S$ :

$$A_c(\alpha_S) = \sum_{n=1}^{\infty} \left( \frac{\alpha_S}{\pi} \right)^n A_c^{(n)} , \quad (10)$$

$$B_c(\alpha_S) = \sum_{n=1}^{\infty} \left( \frac{\alpha_S}{\pi} \right)^n B_c^{(n)} . \quad (11)$$

The structure of the symbolic factor denoted by  $[H^{F=H} C_1 C_2]_{c\bar{c}; a_1 a_2}$  which depends strongly on the initial state channel of the Born subprocess, is explained with detail in Refs. [6, 7]. Here we limit ourselves to the case in which the final state system  $F$  is composed by a single Higgs boson

$$\begin{aligned} [H^{F=H} C_1 C_2]_{gg; a_1 a_2} &= H_g^{F=H}(\alpha_S(M^2)) [C_{g a_1}(z_1; \alpha_S(b_0^2/b^2)) C_{g a_2}(z_2; \alpha_S(b_0^2/b^2)) \\ &+ G_{g a_1}(z_1; \alpha_S(b_0^2/b^2)) G_{g a_2}(z_2; \alpha_S(b_0^2/b^2))] . \end{aligned} \quad (12)$$

The right-hand side of Eq. (12) does not depend on the direction of  $\mathbf{b}$  and this implies that the  $\mathbf{q_T}$  distribution has no azimuthal correlations in the small- $q_T$  region for Higgs boson production [6]. The presence of the  $G_{ga}(z; \alpha_S)$  functions in the right-hand side of Eq. (12) is the manifestation of the helicity-flip contributions. Since in Eq. (12) there are contributions with two  $G_{ga}(z; \alpha_S)$  functions, for Higgs boson production there are only double helicity-flip terms; helicity conservation in the hard-process factor for Higgs boson production forbids contributions that are produced by a single helicity-flip. The helicity-flip  $G_{ga}(z; \alpha_S)$  functions are absent in processes initiated at the Born level by quark annihilation [6]. The gluonic hard-collinear coefficient function  $C_{ga}(z; \alpha_S)$  ( $a = q, \bar{q}, g$ ) in the right-hand side of Eq. (12) has the following perturbative structure

$$C_{ga}(z; \alpha_S) = \delta_{ga} \delta(1-z) + \sum_{n=1}^{\infty} \left( \frac{\alpha_S}{\pi} \right)^n C_{ga}^{(n)}(z) . \quad (13)$$

At variance with Eq. (13), the perturbative expansion of the coefficient functions  $G_{ga}$ , which are specific to gluon-initiated processes, starts at  $\mathcal{O}(\alpha_S)$ , and we write

$$G_{ga}(z; \alpha_S) = \frac{\alpha_S}{\pi} G_{ga}^{(1)}(z) + \sum_{n=2}^{\infty} \left( \frac{\alpha_S}{\pi} \right)^n G_{ga}^{(n)}(z) . \quad (14)$$

The IR finite contribution of the  $n$ -loop correction terms to the Born subprocess are embodied in the hard-virtual function

$$H_g^{F=H}(\alpha_S(M^2)) = 1 + \sum_{n=1}^{\infty} \left( \frac{\alpha_S}{\pi} \right)^n H_g^{F=H(n)}(z_1 p_1, z_2 p_2) . \quad (15)$$

We now turn to the discussion of the resummation scheme dependence of the coefficient functions. The resummation formula (7) is invariant under the following ‘resummation scheme’ transformations [8]:

$$\begin{aligned} H_c^F(\alpha_S) &\rightarrow H_c^F(\alpha_S) [h(\alpha_S)]^{-1} , \\ B_c(\alpha_S) &\rightarrow B_c(\alpha_S) - \beta(\alpha_S) \frac{d \ln h(\alpha_S)}{d \ln \alpha_S} , \\ C_{ab}(\alpha_S, z) &\rightarrow C_{ab}(\alpha_S, z) [h(\alpha_S)]^{1/2} . \end{aligned} \quad (16)$$

The invariance can easily be proven by using the following renormalization-group identity:

$$h(\alpha_S(b_0^2/b^2)) = h(\alpha_S(M^2)) \exp \left\{ - \int_{b_0^2/b^2}^{M^2} \frac{dq^2}{q^2} \beta(\alpha_S(q^2)) \frac{d \ln h(\alpha_S(q^2))}{d \ln \alpha_S(q^2)} \right\} , \quad (17)$$

which is valid for any perturbative function  $h(\alpha_S)$ . Notice that Eq. (17) establishes the evolution of the perturbative functions from the scale  $q^2 = b_0^2/b^2$  to  $q^2 = M^2$ . The QCD  $\beta$  function and its corresponding  $n$ -order  $\beta_n$  coefficient are defined as

$$\frac{d \ln \alpha_S(\mu^2)}{d \ln \mu^2} = \beta(\alpha_S(\mu^2)) = - \sum_{n=0}^{+\infty} \beta_n \left( \frac{\alpha_S}{\pi} \right)^{n+1} . \quad (18)$$

The explicit expression of the first three coefficients [9, 10],  $\beta_0$ ,  $\beta_1$  and  $\beta_2$  are

$$\begin{aligned} \beta_0 &= \frac{1}{12} (11C_A - 2N_f) , & \beta_1 &= \frac{1}{24} (17C_A^2 - 5C_A N_f - 3C_F N_f) , \\ \beta_2 &= \frac{1}{64} \left( \frac{2857}{54} C_A^3 - \frac{1415}{54} C_A^2 N_f - \frac{205}{18} C_A C_F N_f + C_F^2 N_f + \frac{79}{54} C_A N_f^2 + \frac{11}{9} C_F N_f^2 \right) , \end{aligned} \quad (19)$$

where  $N_f$  is the number of QCD massless flavours and the  $SU(N_c)$  colour factors are  $C_A = N_c$  and  $C_F = (N_c^2 - 1)/(2N_c)$ .

The physical origin of the resummation scheme invariance of Eq. (7) is discussed in Ref. [8]. The invariance implies that the hard-virtual factors  $H_c^F, S_c$  (more precisely, the function  $B_c$ ) and  $C_{ab}$  are not unambiguously computable order by order in perturbation theory. After choosing a ‘resummation scheme’, these factors can be unambiguously defined. We rely on the *hard resummation scheme* defined in Ref. [7], which states all the contributions proportional to  $\delta(1 - z)$  are considered in the hard-virtual functions  $H_c^F$ . The precedent condition directly implies that  $H_c^F$  is process dependent whereas the collinear  $C_{ab}$  functions and the resummation coefficients  $B_c$  are independent of the final state system  $F$ .

The truncation of Eq. (7) at a given fixed order requires the explicit use of several resummation coefficients and hard collinear coefficient functions. At NLO, the coefficients  $A_g^{(1)}, B_g^{(1)}, C_{ga}^{(1)}$  ( $a = q, \bar{q}, g$ ) and  $H_g^{H(1)}$  are enough to compute the total cross section and completely differential distributions. Assuming that the Higgs boson couples to a single heavy quark of mass  $m_Q$ , the first-order coefficient  $H_g^{H(1)}$  in the hard scheme is [7]

$$H_g^{H(1)} = C_A \pi^2 / 2 + c_H(m_Q) . \quad (20)$$

The function  $c_H(m_Q)$ , which depends on the NLO virtual corrections of the Born subprocess  $d\sigma_{LO}^F$ , is given in Eq. (B.2) of Ref. [17]. In the limit  $m_Q \rightarrow \infty$ , the function  $c_H$  becomes

$$c_H(m_Q) \longrightarrow \frac{5C_A - 3C_F}{2} = \frac{11}{2} . \quad (21)$$

Therefore the complete NLO set of necessary coefficients to compute Higgs boson production, in the limit in which the mass of the heavy quark  $Q$  (the top quark  $Q = t$ ) is larger than any other scale involved in the process ( $M_H \ll m_t$ ) is

$$\begin{aligned} A_g^{(1)} &= C_A , & B_g^{(1)} &= -\frac{1}{6} (11C_A - 2N_f) , & H_g^{H(1)} &= \frac{1}{2} (11 + C_A \pi^2) , \\ C_{ga}^{(1)}(z) &= \frac{1}{2} C_F z & [a = q, \bar{q}] , & & C_{gg}^{(1)}(z) &= 0 . \end{aligned} \quad (22)$$

The coefficients  $A_g^{(1)}$  and  $B_g^{(1)}$  are process independent, but even more, they are resummation scheme independent. In the hard resummation scheme the collinear functions  $C_{ga}^{(1)}$  ( $a = q, \bar{q}, g$ ) are process independent whereas  $H_g^{H(1)}$  depends on final state system ( $F = H$ ), and both depend on the resummation scheme in such a way to ensure the resummation scheme independence of Eq. (7) at NLO. The computation of the hard-virtual coefficients  $H_c^{H(1)}$  requires a particular prescription which is known from some time [11]. The explicit calculations and the results of Ref. [11] show that the NLO hard-virtual coefficient  $H_c^{F(1)}$  is explicitly related in a process-independent form to  $d\hat{\sigma}_{\text{LO}}^F$  and to the IR finite part of the NLO virtual correction to the Born cross section. The precedent process-independent relation is based on the definition of universal subtraction operators that cancel the IR divergences of the one-loop (NLO) virtual correction to the Born cross section and fix the first order IR finite constant  $\delta_{q_T}$  [7]. The coefficient  $\delta_{q_T}$ , that only depends on the initial state partons, has a *soft* origin and it is defined in Refs. [11] and [7].

At NNLO, the coefficients  $A_g^{(2)}$  and  $B_g^{(2)}$  are needed,

$$A_g^{(2)} = \frac{1}{2} C_A \left[ \left( \frac{67}{18} - \frac{\pi^2}{6} \right) C_A - \frac{5}{9} N_f \right] , \quad B_g^{(2)} = \frac{\gamma_{g(1)}}{16} + \beta_0 C_A \zeta_2 , \quad (23)$$

where  $\gamma_{g(1)}$  is the coefficient of the  $\delta(1-z)$  term in the NLO gluon splitting functions [14, 15], which reads

$$\gamma_{g(1)} = \left( -\frac{64}{3} - 24\zeta_3 \right) C_A^2 + \frac{16}{3} C_A N_f + 4 C_F N_f , \quad (24)$$

and  $\zeta_n$  is the Riemann zeta-function ( $\zeta_2 = \pi^2/6, \zeta_3 = 1.202\dots, \zeta_4 = \pi^4/90$ ). The coefficient  $A_g^{(2)}$  does not depend on the resummation scheme whereas  $B_g^{(2)}$  in Eq. (23) is expressed in the hard resummation scheme and both coefficients are process independent. The collinear functions  $C_{ga}^{(2)}$  ( $a = q, \bar{q}, g$ ) in the hard resummation scheme can be extracted from Refs. [7, 12] and they are independent of the final state system  $F$ .

The general structure of the hard-virtual coefficients  $H_c^F$  is known only recently [7]. Although this factor is process dependent, in Ref. [7] was shown that it can be directly related in a universal (process-independent) way to the IR finite part of the all-order virtual amplitude of the corresponding partonic subprocess  $c\bar{c} \rightarrow F$ . The precedent relation between  $H_c^F$  and the all-order virtual correction to the partonic subprocess  $c\bar{c} \rightarrow F$  is explicitly known up to the NNLO and it is based on the definition of universal subtraction operators that cancel the IR divergences of the two-loop (NNLO) virtual corrections to the Born cross section. These universal second order operators contain an IR finite term of soft origin ( $\delta_{q_T}^{(1)}$ ) that only depends on the initial state partons [7].

In the case of Higgs boson production the hard-virtual factor  $H_g^{F=H(2)}$  in the large- $m_t$  limit (in the hard scheme) is [12]

$$\begin{aligned} H_g^{H(2)} = & C_A^2 \left( \frac{3187}{288} + \frac{7}{8} L_t + \frac{157}{72} \pi^2 + \frac{13}{144} \pi^4 - \frac{55}{18} \zeta_3 \right) + C_A C_F \left( -\frac{145}{24} - \frac{11}{8} L_t - \frac{3}{4} \pi^2 \right) \\ & + \frac{9}{4} C_F^2 - \frac{5}{96} C_A - \frac{1}{12} C_F - C_A N_f \left( \frac{287}{144} + \frac{5}{36} \pi^2 + \frac{4}{9} \zeta_3 \right) + C_F N_f \left( -\frac{41}{24} + \frac{1}{2} L_t + \zeta_3 \right) , \end{aligned} \quad (25)$$

where  $L_t = \ln(M^2/m_t^2)$ . The two-loop scattering amplitude [16] used in the computation of  $H_g^{F=H(2)}$  includes corrections to the large- $m_t$  approximation (the evaluation of the corrections uses the expansion parameter  $1/m_t^2$ ). At NNLO, in Eq. (12) (which is proportional to  $\delta(q_T^2)$ ) the first order  $G_{ga}^{(1)}$  helicity-flip functions are also needed and they read [6]

$$G_{ga}^{(1)}(z) = C_a \frac{1-z}{z} \quad a = q, \bar{q}, g. \quad (26)$$

The first-order functions  $G_{ga}^{(1)}$  are resummation-scheme independent and they do not depend on the final state system  $F$ .

At N<sup>3</sup>LO, the numerical implementation of Eq. (7) requires the following ingredients:  $A_g^{(3)}$ ,  $B_g^{(3)}$ ,  $C_{ga}^{(3)}$  ( $a = q, \bar{q}, g$ ) and  $H_g^{H(3)}$ . The coefficient  $A_c^{(3)}$  [21] reads

$$\begin{aligned} A_c^{(3)} = & \frac{1}{4} C_c \left\{ C_A^2 \left( \frac{245}{24} - \frac{67}{9} \zeta_2 + \frac{11}{6} \zeta_3 + \frac{11}{5} \zeta_2^2 \right) + C_F n_f \left( -\frac{55}{24} + 2\zeta_3 \right) \right. \\ & \left. + C_A n_f \left( -\frac{209}{108} + \frac{10}{9} \zeta_2 - \frac{7}{3} \zeta_3 \right) - \frac{1}{27} n_f^2 \right\} + \frac{1}{8} \beta_0 C_c \left( C_A \left( \frac{808}{27} - 28\zeta_3 \right) - \frac{224}{54} n_f \right). \end{aligned} \quad (27)$$

The explicit expression of the  $B_c^{(3)}$  ( $a = q, g$ ) coefficients in the hard scheme can be computed from Refs. [18, 19]. In the particular case of the gluon channel we have

$$\begin{aligned} B_g^{(3)} = & -\frac{2133}{64} + \frac{3029}{576} N_f - \frac{349}{1728} N_f^2 + \frac{109}{6} \pi^2 - \frac{283}{144} \pi^2 N_f + \frac{5}{108} \pi^2 N_f^2 - \frac{253}{160} \pi^4 + \frac{23}{240} \pi^4 N_f \\ & - \frac{843}{8} \zeta_3 + 2\zeta_3 N_f + \frac{1}{6} \zeta_3 N_f^2 + \frac{9}{4} \pi^2 \zeta_3 + \frac{135}{2} \zeta_5. \end{aligned} \quad (28)$$

The analytical form of the function  $\Sigma^{F(3)}$  in Eq. (7) is completely known and the subtraction of the divergencies can be performed at N<sup>3</sup>LO without any approximation. Nevertheless, the general structure of the coefficient  $\mathcal{H}^{F(3)}$  (which is proportional to  $\delta(q_T^2)$ ) is not known in analytic form for any hard-scattering process. Nonetheless, within our subtraction formalism,  $\mathcal{H}^{F(3)}$  can be determined for any hard-scattering process whose corresponding total cross section is known at N<sup>3</sup>LO. This point is discussed in detail in Sect. 3.

At N<sup>3</sup>LO the universal relation between  $H_c^{F(3)}$  and the third-order virtual correction to the partonic subprocess  $c\bar{c} \rightarrow F$  presents one missing ingredient: the *single* coefficient (of *soft* origin) that appear in the finite part of the structure of the IR singularities of the third-order virtual amplitude of the corresponding partonic subprocess  $c\bar{c} \rightarrow F$ . Although a general prescription to compute analytically the hard-virtual coefficient  $H_g^{H(3)}$  is not completely known, using the corresponding hard-virtual factor  $C_{gg \rightarrow H}^{\text{th}(3)}$  [20] for threshold resummation (in the large- $m_t$  limit) and the exponential equation that relates threshold and  $q_T$  resummation hard-virtual coefficients

(Eq. (81) of Ref. [7]), we compute the following approximated expression

$$\begin{aligned}
\tilde{H}_g^{H(3)} = & C_A^3 \left( -\frac{15649\zeta_3}{432} - \frac{121\pi^2\zeta_3}{432} + \frac{3\zeta_3^2}{2} + \frac{869\zeta_5}{144} + \frac{215131}{5184} + \frac{16151\pi^2}{7776} - \frac{961\pi^4}{15552} + \frac{\pi^6}{810} \right. \\
& + \frac{105}{32}\zeta_6 \Big) + C_A^2 \left( \frac{605\zeta_3}{72} + \frac{55\pi^2\zeta_3}{36} + \frac{737\pi^2}{432} + \frac{167\pi^4}{432} + \frac{\pi^6}{72} \right) \\
& + C_A \left( \frac{19\pi^2 L_t}{48} - \frac{55\pi^2\zeta_3}{8} - \frac{\pi^6}{480} + \frac{133\pi^4}{72} + \frac{11399\pi^2}{864} + \frac{63}{32}\zeta_6 \right) \\
& + N_f^2 \left( \frac{43C_A\zeta_3}{108} - \frac{19\pi^4 C_A}{3240} - \frac{133\pi^2 C_A}{1944} + \frac{2515C_A}{1728} - \frac{7C_F\zeta_3}{6} \right. \\
& + \frac{4481C_F}{2592} - \frac{\pi^4 C_F}{3240} - \frac{23\pi^2 C_F}{432} \Big) \\
& + N_f \left( \frac{101C_A^2\zeta_5}{72} - \frac{97}{216}\pi^2 C_A^2\zeta_3 + \frac{29C_A^2\zeta_3}{8} + \frac{1849\pi^4 C_A^2}{38880} - \frac{35\pi^2 C_A^2}{243} - \frac{98059C_A^2}{5184} \right. \\
& + \frac{5C_A C_F\zeta_5}{2} + \frac{13C_A C_F\zeta_3}{2} + \frac{1}{2}\pi^2 C_A C_F\zeta_3 - \frac{63991C_A C_F}{5184} + \frac{11\pi^4 C_A C_F}{6480} - \frac{71}{216}\pi^2 C_A C_F \\
& + \frac{1}{9}\pi^2 C_A L_t - \frac{5}{36}\pi^2 C_A\zeta_3 - \frac{55C_A\zeta_3}{36} - \frac{5\pi^4 C_A}{54} - \frac{1409\pi^2 C_A}{864} \\
& \left. - 5C_F^2\zeta_5 + \frac{37C_F^2\zeta_3}{12} + \frac{19C_F^2}{18} \right) . \tag{29}
\end{aligned}$$

Notice that we neglect all the third order terms in the exponent of Eq. (81) in Ref. [7], considering the entire  $\mathcal{O}(\alpha_s^3)$  correction (in the exponent) as unknown. The  $\tilde{H}_g^{H(3)}$  coefficient in Eq. (29) will be used in the numerical computations in the present paper. Finally the collinear functions  $C_{ga}^{(3)}$  ( $a = q, \bar{q}, g$ ) and the second-order helicity-flip functions  $G_{ga}^{(2)}$  (which are universal) are not known.

### 3 The Higgs boson total cross section at N<sup>3</sup>LO

We start this section with some observations related to the hard-scattering function  $\mathcal{H}_{c\bar{c}\leftarrow ab}^F$ . This function is resummation-scheme independent, but it depends on the specific hard-scattering subprocess  $c + \bar{c} \rightarrow F$ . The coefficients  $\mathcal{H}_{c\bar{c}\leftarrow ab}^{F(n)}$  of the perturbative expansion in Eq. (6) can be determined by performing a customary perturbative calculation of the  $q_T$  distribution in the limit  $q_T \rightarrow 0$ . In right-hand side of Eq. (7), within our subtraction method, the function  $\mathcal{H}^F$  controls the strict perturbative normalization of the corresponding total cross section (i.e. the integral of the total  $q_T$  distribution). This unitary-related property can be exploited to determine the coefficients  $\mathcal{H}_{c\bar{c}\leftarrow ab}^{F(n)}$  from the perturbative calculation of the total cross section. At the partonic level, the integral of the total  $q_T$  distribution in Eq. (3) results in the total cross section  $\hat{\sigma}_{Fab}^{\text{tot}}$ ,

$$\hat{\sigma}_{Fab}^{\text{tot}}(M, \hat{s}; \alpha_s(\mu_R^2), \mu_R^2, \mu_F^2) = \int_0^\infty dq_T^2 \frac{d\hat{\sigma}_{Fab}}{dq_T^2}(q_T, M, \hat{s}; \alpha_s(\mu_R^2), \mu_R^2, \mu_F^2) . \tag{30}$$

Since the the hard-scattering function  $\mathcal{H}_{c\bar{c}\leftarrow ab}^F$  is simply proportional to  $\delta(q_T^2)$ , we evaluate the  $q_T$  spectrum on right-hand side of Eq. (3) according to the following decomposition

$$\hat{\sigma}_{Fab}^{\text{tot}} = \frac{M^2}{\hat{s}} \mathcal{H}_{ab}^F + \int_0^\infty dq_T^2 \frac{d\hat{\sigma}_{Fab}^{(\text{fin.})}}{dq_T^2} , \tag{31}$$



where  $d\hat{\sigma}_{Fab}^{(\text{fin.})}$  is directly related to the quantity in square bracket in the right-hand side of Eq. (3)

$$\frac{d\hat{\sigma}_{Fab}^{(\text{fin.})}}{dq_T^2} \equiv \left[ \frac{d\hat{\sigma}_{ab}^{F+\text{jets}}}{dq_T^2} - \frac{d\hat{\sigma}_{ab}^{F \text{ CT}}}{dq_T^2} \right]. \quad (32)$$

The relation in Eq. (31) is valid order by order in QCD perturbation theory. Once the perturbative coefficients of the fixed-order expansions of  $\hat{\sigma}_{Fab}^{\text{tot}}$ ,  $\mathcal{H}_{ab}^F$  and  $d\hat{\sigma}_{Fab}^{(\text{fin.})}/dq_T^2$  are all known, the relation (31) has to be regarded as an identity, which can explicitly be checked. Note, however, that since the fixed-order truncation  $d\hat{\sigma}_{Fab}^{(\text{fin.})}/dq_T^2$  does not contain any contributions proportional to  $\delta(q_T^2)$ ,  $[d\hat{\sigma}_{Fab}^{(\text{fin.})}/dq_T^2]_{\text{NLO}}$  does not explicitly depend on the coefficient  $\mathcal{H}_{ab}^{F(1)}$ . Analogously,  $[d\hat{\sigma}_{Fab}^{(\text{fin.})}/dq_T^2]_{\text{NNLO}}$  does not explicitly depend on the coefficient  $\mathcal{H}_{ab}^{F(2)}$ , and so forth. Therefore, Eq. (31) can be used to determine the  $N^n\text{LO}$  coefficient  $\mathcal{H}_{ab}^{F(n)}$  from the knowledge of  $\hat{\sigma}_{Fab}^{\text{tot}}$  at  $N^n\text{LO}$  and of  $d\hat{\sigma}_{Fab}^{(\text{fin.})}/dq_T^2$  at  $N^n\text{LO}$ , without the need of explicitly computing the small- $q_T$  behaviour of the spectrum  $d\hat{\sigma}_{Fab}/dq_T^2$  at  $N^n\text{LO}$ . For example, at  $N^3\text{LO}$  Eq. (31) reads

$$\begin{aligned} & \left(\frac{\alpha_S}{\pi}\right)^3 \frac{M^2}{\hat{s}} \sum_c \sigma_{c\bar{c},F}^{(0)}(\alpha_S, M) \mathcal{H}_{c\bar{c} \leftarrow ab}^{F(3)} \left( \frac{M^2}{\hat{s}}; \frac{M^2}{\mu_R^2}, \frac{M^2}{\mu_F^2}, \frac{M^2}{Q^2} \right) \\ &= \left\{ \left[ \hat{\sigma}_{Fab}^{\text{tot}} \right]_{N^3\text{LO}} - \left[ \hat{\sigma}_{Fab}^{\text{tot}} \right]_{\text{NNLO}} \right\} - \int_0^\infty dq_T^2 \left\{ \left[ \frac{d\hat{\sigma}_{Fab}^{(\text{fin.})}}{dq_T^2} \right]_{N^3\text{LO}} - \left[ \frac{d\hat{\sigma}_{Fab}^{(\text{fin.})}}{dq_T^2} \right]_{\text{NNLO}} \right\}, \quad (33) \end{aligned}$$

where  $\alpha_S = \alpha_S(\mu_R^2)$  and we have used

$$\left[ \hat{\sigma}_{Fab}^{\text{tot}}(M, \hat{s}; \alpha_S) \right]_{\text{LO}} = \delta(1 - M^2/\hat{s}) \sum_c \sigma_{c\bar{c},F}^{(0)}(\alpha_S, M) \delta_{ca} \delta_{\bar{c}b}. \quad (34)$$

The generalization at any order  $n$  ( $n > 1$ ) is [2]

$$\begin{aligned} \left(\frac{\alpha_S}{\pi}\right)^n \frac{M^2}{\hat{s}} \sum_c \sigma_{c\bar{c},F}^{(0)}(\alpha_S, M) \mathcal{H}_{c\bar{c} \leftarrow ab}^{F(n)} &= \left\{ \left[ \hat{\sigma}_{Fab}^{\text{tot}} \right]_{N^n\text{LO}} - \left[ \hat{\sigma}_{Fab}^{\text{tot}} \right]_{N^{n-1}\text{LO}} \right\} \\ &- \int_0^\infty dq_T^2 \left\{ \left[ \frac{d\hat{\sigma}_{Fab}^{(\text{fin.})}}{dq_T^2} \right]_{N^n\text{LO}} - \left[ \frac{d\hat{\sigma}_{Fab}^{(\text{fin.})}}{dq_T^2} \right]_{N^{n-1}\text{LO}} \right\}. \quad (35) \end{aligned}$$

At LO, where only the Born subprocess is available,  $\left[ \frac{d\hat{\sigma}_{Fab}^{(\text{fin.})}}{dq_T^2} \right]_{\text{LO}}$  is identically zero by definition. If all the components in right-hand side of Eq. (35) are known analytically (as it was the case at NNLO in Refs. [12, 13]) the function  $\mathcal{H}_{ab}^F$  can be extracted exactly in analytical form. At NLO the extraction of the function  $\mathcal{H}_{ab}^{F(1)}$  is straightforward for Drell-Yan and Higgs boson production. The function  $\mathcal{H}_{ab}^{F(2)}$  at NNLO (for Higgs ( $F = H$ ) boson production [12] and Drell-Yan ( $F = DY$ ) [13]) can be obtained with a dedicated analytical computation using Eq. (35) for  $n = 2$ . Since for Higgs boson production, the transverse momentum cross section  $H+\text{jet}$  at NNLO is not known analytically, Eq. (33) can be used only numerically in the computation of the function  $\mathcal{H}_{ab}^{F(3)}$ .

The following paragraphs will be used to explain in detail the degree of approximation that is intended to use. Instead of compute the entire third order function  $\mathcal{H}_{ab}^{H(3)}$  numerically (which is not recommended) we first report all its ingredients with the aim of reduce the numerical extraction

to only a few components (perturbative functions). With this purpose, using Eqs. (7) and (12) we define

$$\mathcal{H}_{gg \leftarrow ab}^H(z; \alpha_S) \equiv H_g^H(\alpha_S) \int_0^1 dz_1 \int_0^1 dz_2 \delta(z - z_1 z_2) \left[ C_{ga}(z_1; \alpha_S) C_{gb}(z_2; \alpha_S) + G_{ga}(z_1; \alpha_S) G_{gb}(z_2; \alpha_S) \right]. \quad (36)$$

There are only two differences between Eqs. (12) and (36). The first difference is due to the fact that the function  $\mathcal{H}^H$  depends on the energy fraction  $z$ , since the right-hand side of Eq. (36) involves a convolution integral over the momentum fractions  $z_1$  and  $z_2$ . The second difference regards the scale of  $\alpha_S$ : in the functions  $H^H(\alpha_S)$ ,  $C(\alpha_S)$  and  $G(\alpha_S)$  on the right-hand side of Eq. (36), the argument of  $\alpha_S$  is set to the same value (this common scale is not explicitly denoted in Eq. (36)). Owing to this feature, the process-dependent function  $\mathcal{H}_{gg \leftarrow ab}^H$  is unambiguously defined (i.e., it is independent of the specification of the resummation scheme) [8]. The  $\mathcal{H}^H$  function in Eq. (36) can be expanded perturbatively without approximation at any order in the strong coupling constant  $\alpha_S$ . The perturbative expansion of the function  $\mathcal{H}^H$  directly follows from Eqs. (13)–(15) and for the first-order and second-order contributions we have

$$\mathcal{H}_{gg \leftarrow ab}^{H(1)}(z) = \delta_{ga} \delta_{gb} \delta(1 - z) H_g^{H(1)} + \delta_{ga} C_{gb}^{(1)}(z) + \delta_{gb} C_{ga}^{(1)}(z) , \quad (37)$$

$$\begin{aligned} \mathcal{H}_{gg \leftarrow ab}^{H(2)}(z) = & \delta_{ga} \delta_{gb} \delta(1 - z) H_g^{H(2)} + \delta_{ga} C_{gb}^{(2)}(z) + \delta_{gb} C_{ga}^{(2)}(z) + H_g^{H(1)} \left( \delta_{ga} C_{gb}^{(1)}(z) + \delta_{gb} C_{ga}^{(1)}(z) \right) \\ & + \left( C_{ga}^{(1)} \otimes C_{gb}^{(1)} \right)(z) + \left( G_{ga}^{(1)} \otimes G_{gb}^{(1)} \right)(z) . \end{aligned} \quad (38)$$

In Eq. (38) and in the following, the symbol  $\otimes$  denotes the convolution integral (i.e., we define  $(g \otimes h)(z) \equiv \int_0^1 dz_1 \int_0^1 dz_2 \delta(z - z_1 z_2) g(z_1) h(z_2)$ ). The new third-order contribution is

$$\begin{aligned} \mathcal{H}_{gg \leftarrow ab}^{H(3)}(z) = & \delta_{ga} \delta_{gb} \delta(1 - z) H_g^{H(3)} + \delta_{ga} C_{gb}^{(3)}(z) + \delta_{gb} C_{ga}^{(3)}(z) + H_g^{H(1)} \left( \delta_{ga} C_{gb}^{(2)}(z) + \delta_{gb} C_{ga}^{(2)}(z) \right) \\ & + H_g^{H(2)} \left( \delta_{ga} C_{gb}^{(1)}(z) + \delta_{gb} C_{ga}^{(1)}(z) \right) + \left( C_{ga}^{(1)} \otimes C_{gb}^{(2)} \right)(z) + \left( C_{ga}^{(2)} \otimes C_{gb}^{(1)} \right)(z) \\ & + \left( G_{ga}^{(1)} \otimes G_{gb}^{(2)} \right)(z) + \left( G_{ga}^{(2)} \otimes G_{gb}^{(1)} \right)(z) + H_g^{H(1)} \left( C_{ga}^{(1)} \otimes C_{gb}^{(1)} \right)(z) \\ & + H_g^{H(1)} \left( G_{ga}^{(1)} \otimes G_{gb}^{(1)} \right)(z) . \end{aligned} \quad (39)$$

The perturbative functions  $C_{ga}^{(1)}(z)$ ,  $C_{ga}^{(2)}(z)$ ,  $G_{ga}^{(1)}(z)$ ,  $H_g^{H(1)}$  and  $H_g^{H(2)}$  are reported in Sec. 2, and therefore the coefficient functions  $\mathcal{H}^{H(1)}$  and  $\mathcal{H}^{H(2)}$  are known analytically. As stated in Sec. 2, the second-order helicity-flip functions  $G_{ga}^{(2)}(z)$  and the third-order collinear functions  $C_{ga}^{(3)}(z)$  are not known implying that the third order  $\mathcal{H}^{H(3)}$  function can only be obtained numerically. In addition, the third-order hard-virtual coefficient  $H_g^{H(3)}$  is not fully analytical determined. The missing terms in Eq. (29), concerning the final expression of  $H_g^{H(3)}$ , have a *soft* origin. Following notation of Ref. [7], all the third order terms in the right hand side in Eq. (81) of Ref. [7] are denoted by  $\delta_{(2)}^{qT}$ . This allows to perform a subsequent decomposition for the third order hard-virtual coefficient defined in Eq. (29)

$$\tilde{H}_g^{H(3)} \equiv H_g^{H(3)} - [H_g^{H(3)}]_{(\delta_{(2)}^{qT})} . \quad (40)$$

Therefore the numerical extraction is constrained to the functions  $G_{ga}^{(2)}(z)$ ,  $C_{ga}^{(3)}(z)$  and  $[H_g^{H(3)}]_{(\delta_{(2)}^{q_T})}$ . A naïve numerical implementation of Eq. (33) results in the following approximation

$$C_{N3} \delta_{ga} \delta_{gb} \delta(1-z) \leftarrow \delta_{ga} \delta_{gb} \delta(1-z) [H_g^{H(3)}]_{(\delta_{(2)}^{q_T})} + \delta_{ga} C_{gb}^{(3)}(z) + \delta_{gb} C_{ga}^{(3)}(z) \\ + \left( G_{ga}^{(1)} \otimes G_{gb}^{(2)} \right)(z) + \left( G_{ga}^{(2)} \otimes G_{gb}^{(1)} \right)(z) , \quad (41)$$

where the third-order numerical coefficient  $C_{N3}$  embodies the numerical extraction of the hard-virtual coefficient  $H_g^{H(3)}(\delta_{(2)}^{q_T})$  *plus* the numerical reduction of a function of the variable  $z$  to a numerical term proportional to  $\delta(1-z)$ . The resulting numerical coefficient  $[H_g^{H(3)}]_{(\delta_{(2)}^{q_T})}$  is exact since  $C_{N3}$  is proportional to  $\delta(1-z)$ . The approximation that implies Eq. (41) is related only to the functions  $G_{ga}^{(2)}(z)$  and  $C_{ga}^{(3)}(z)$ , which their functional dependence on the variable  $z$  goes beyond  $\delta(1-z)$ .

The method proposed in Eq. (41) to approximate numerically unknown terms in the hard-virtual function  $\mathcal{H}_{gg \leftarrow ab}^H(z)$  is not new. It was first used in Ref. [2] in order to compute numerically the second order function  $\mathcal{H}_{gg \leftarrow ab}^{H(2)}(z)$  at NNLO, providing a reasonable estimate of the exact result to better than 1% accuracy. Notice that Eq. (41) allows to recover the total cross section (at N<sup>3</sup>LO in this case) with no approximation. After integration over the transverse momentum  $q_T$ , Eq. (30) provides the same total integral (numerically in this case) that in the fully analytical case. Even more, for IR observables (at fixed order) which verify that the *back-to-back* kinematical region ( $q_T = 0$ ) is located in a single phase space point (e.g the  $q_T$  distribution, the angular separation  $\Delta\Phi_{\gamma\gamma}$  between the two photons for a Higgs boson decaying into diphotons, etc.), we consider our fixed order result as with no approximation, i.e, the integral of the analytical unknown terms in Eq. (41) (which all have  $q_T = 0$ ) are located in one single point of the exclusive differential distributions.

In Sec. 4.1 we perform a detailed numerical study, of the proposed approximation in Eq. (41), but at one order less (NNLO), showing that even for the rapidity distribution, the approximated result differs less than 1% in kinematical regions where the bulk of the cross section takes place.

### 3.1 The numerical computation of $C_{N3}$

Now we turn the discussion to the numerical extraction of the coefficient  $C_{N3}$  using Eqs. (39), (29) and (33).

In the numerical studies performed in this Section and in the differential predictions presented in Sections 4.1, 4.2 and 5, we consider the Higgs boson production in  $pp$  collisions at the centre-of-mass energy  $\sqrt{s} = 13$  TeV. We use the Higgs boson mass  $M_H = 125$  GeV and the vacuum expectation value  $v = 246.2$  GeV. Higgs production in gluon fusion is mediated through a heavy top quark loop. If all scales involved in the process under consideration are substantially smaller than the top quark mass, it is possible to integrate out the top quark loop by taking the large- $m_t$  limit ( $m_t \rightarrow \infty$ ). The mass of the top quark is taken  $m_t = 173.2$  GeV in those contributions which do not vanish in the large- $m_t$  limit (e.g Eqs. (25) and (29)). We use the central member of the PDF4LHC15 parton distribution functions (PDFs) [22] as implemented in the LHAPDF framework [24] and the associated strong coupling constant  $\alpha_s$ . Note that we systematically employ the same

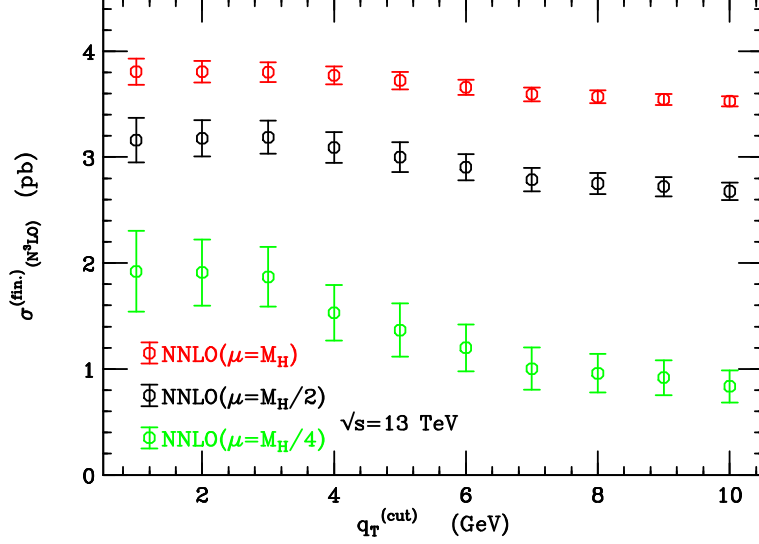


Figure 1: The  $q_T$  integrated finite contribution to the cross section of Eq. (32) at  $\text{N}^3\text{LO}$  exclusively (i.e.  $\text{N}^3\text{LO}$ -NNLO) between  $q_T^{\text{cut}}$  and  $\infty$ , for three different scales  $\mu = \mu_R = \mu_F$ .

order of the PDFs (NNLO) for the LO, NLO, NNLO and  $\text{N}^3\text{LO}$  results presented in this paper. The default factorization and renormalization scales are chosen accordingly to  $\mu \equiv \mu_R = \mu_F = M_H/2$ . The theoretical uncertainty is estimated by varying the default scale choice by a factor  $\{1/2, 2\}$ .

The numerical implementation of the  $q_T$  subtraction formalism of Eq. (3) makes use of the cross section  $d\hat{\sigma}_{ab}^{H+\text{jets}}$  up to NNLO, which is implemented in the parton-level Monte Carlo generator NNLOJET [23]. This program provides the necessary infrastructure for the antenna subtraction [4] of hadron collider processes at NNLO and performs the integration of all contributing subprocesses of the type  $d\hat{\sigma}_{ab}^{H+\text{jets}}$  at this order. The counter term and the hard function  $\mathcal{H}^H$  are encoded in a new Monte Carlo generator HN3LO up to the third order in the strong coupling constant. All our results up-to the NNLO are in accord with the Monte Carlo generator HNNLO [1] at the per mille level of accuracy.

In the numerical implementation of Eq. (33), the lower bound of the  $q_T$  integral ( $q_T = 0$ ) has to be replaced with a suitable choice of the  $q_T^{\text{cut}}$ . The resulting  $\hat{\sigma}_{Fab}^{(\text{fin.})}$  integral has to be  $q_T^{\text{cut}}$  independent within the statistical uncertainties. In Fig. 1 we report the  $\sigma_{Fab}^{(\text{fin.})}$  (i.e.  $\hat{\sigma}_{Fab}^{(\text{fin.})}$  convoluted with the parton distribution functions) cross section at  $\text{N}^3\text{LO}$  exclusively as a function of the  $q_T^{\text{cut}}$ . With  $\text{N}^3\text{LO}$  exclusively we understand  $\left[\sigma_{Fab}^{(\text{fin.})}\right]_{\text{N}^3\text{LO}} - \left[\sigma_{Fab}^{(\text{fin.})}\right]_{\text{NNLO}}$ .

Using Eq. (39) with Eq. (33) and the value of the resulting integral  $\sigma_{Fab}^{(\text{fin.})}(q_T^{\text{cut}} = 1 \text{ GeV})$  in Fig. 1, it is possible to obtain the  $q_T$  integrated cross section of the unknown terms in the right hand side of Eq. (41) and consequently  $C_{N3}$ . The behaviour of the  $\text{N}^3\text{LO}$   $\sigma_{Fab}^{(\text{fin.})}$  cross section as a function of  $q_T^{\text{cut}}$  in Fig. 1 allows also to estimate the systematical uncertainty corresponding to the use of this technical cut. In Fig. 2 we show the  $C_{N3}$  predicted value for each scale (in black points). Notice that the central value of each predicted  $C_{N3}$  is independent of the scale (within the uncertainties), in complete agreement with Eq. (39). The scale independence of  $C_{N3}$  is not related with the used ansatz of Eq. (41). The terms in the right-hand side of Eq. (39) are all

scale independent and the relation between  $C_{N3}$  and  $\tilde{H}_g^{H(3)}$  is univocal defined considering Eqs. (39), (40) and (41).

The black error bars for each one of the  $C_{N3}$  values are calculated with the conventional propagation of the uncertainties and it is almost entirely due to the size of the uncertainties of the N<sup>3</sup>LO  $\sigma_{Fab}^{(fin.)}$  cross section in Fig. 1.

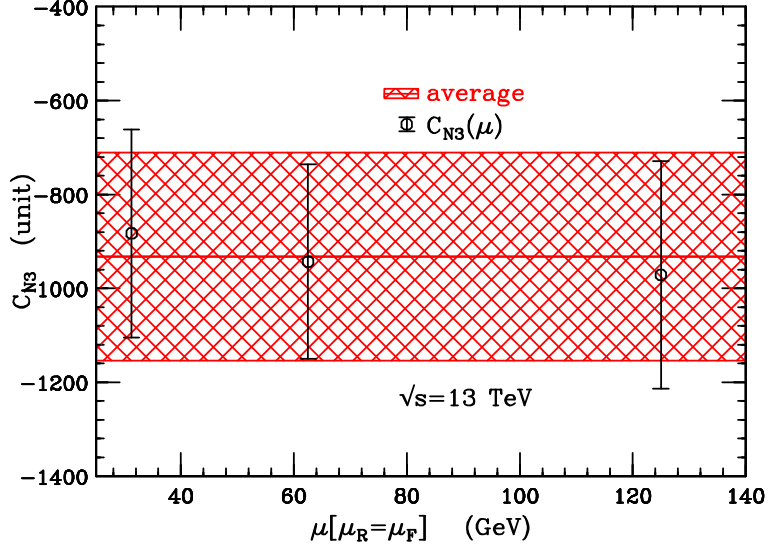


Figure 2: The numerically computed  $C_{N3}$  coefficient as defined in Eq. (41) (black points) for the particular case of  $q_T^{cut} = 1$  GeV. The black error bars for each  $C_{N3}$  point is obtained propagating the statistical uncertainties of the different terms involved in the computation. The red band is calculated with the average of the three particular  $C_{N3}$  values for each scale as detailed in the text.

The solid red central line in Fig. 2, is the average value calculated with the three different black points corresponding to each scale choice, whereas the red band is the predicted uncertainty. The value of the resulting coefficient using the three scales presented in Fig. 2 is  $C_{N3} = -932 \pm 222$ . Besides the precedent cited three central scales we also present predictions for other four scales that complete a seven-point scale variation varying the default scale choice ( $M_H/2$ ) by a factor  $\{1/2, 2\}$ . In Fig. (3) we show the computed  $C_{N3}$  coefficients corresponding to each one of the seven scales as a function of the label of the scale as stated in Table 1. The red band and central value (red line) is calculated with the first three black points at  $q_T^{cut} = 1$  GeV already present in Fig. 2 and detailed in Table 1 in bold typeface. In Fig. (3) we also compare the computed  $C_{N3}$  coefficients at  $q_T^{cut} = 1$  GeV with the cases in which  $q_T^{cut} = 2$  GeV (blue points) and 3 GeV (green points) are used. The variation of the  $q_T^{cut}$  around 2 GeV quantifies the stability of the  $C_{N3}$  extraction. Whereas the  $C_{N3}$  coefficient is independent of the scale choice its resulting cross section, after convolution with the PDFs (which depend on  $\mu_F$ ) and the strong coupling constant  $\alpha_S(\mu_R)$ , does depend on the scale choice. In Table 1 we present all the  $C_{N3}$  coefficients as a function of the scale choice and the  $q_T^{cut}$  ( $q_T^{cut} = 2 \pm 1$  GeV).

The numerically calculated  $C_{N3}$  coefficient allows to predict the total cross section at N<sup>3</sup>LO within the transverse momentum subtraction method (as well completely differential distributions). In Fig. 4 we compare the fully analytical N<sup>3</sup>LO Higgs boson total cross section [25] (black

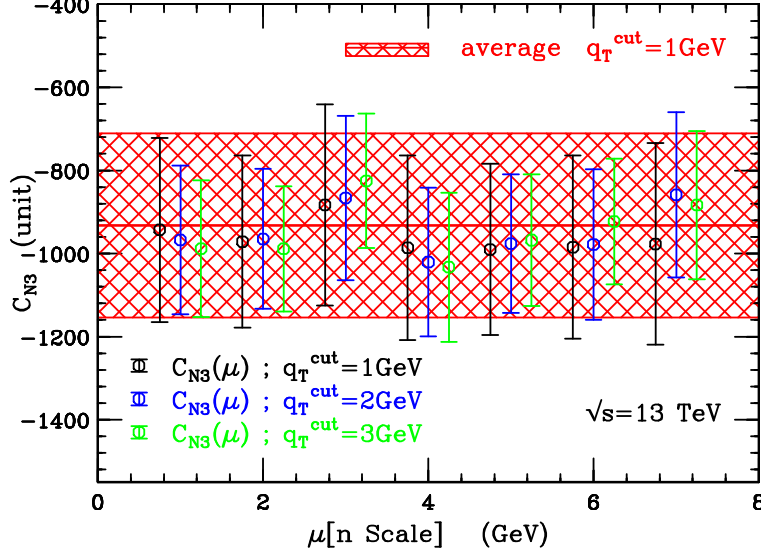


Figure 3: *The numerically computed  $C_{N3}$  coefficient (for three different values of  $q_T^{cut}$ ) as a function of the number of the scale as detailed in Table 1. The error bars for each particular  $C_{N3}$  point is obtained propagating the statistical uncertainties of the different terms involved in the computation. The red band is calculated with the average of the three particular  $C_{N3}$  values of the three scales present in Fig. 2 at  $q_T^{cut} = 1$  GeV, as detailed in the text.*

points) and our best estimation (green points) for three central scales, using  $q_T^{cut} = 1$  GeV. The blue squared points constitute our best approximation without the use of the  $C_{N3}$  coefficient (i.e.  $C_{N3} = 0$ ), that can be considered as the prediction of the  $q_T$  subtraction method in the case in which the total cross section is unknown (e.g. for Drell-Yan at N<sup>3</sup>LO). The uncertainty bars in the  $q_T$  subtraction prediction correspond to the statistical errors of the numerical computation and are mainly due to the finite contribution in Eq. (32) at N<sup>3</sup>LO exclusively. The magenta and cyan points correspond to our N<sup>3</sup>LO prediction using  $q_T^{cut} = 2$  GeV and 3 GeV respectively. Notice that the  $q_T^{cut}$  variation is performed at N<sup>3</sup>LO exclusively, while the NNLO cross section is not varied over the different  $q_T^{cut}$  parameters. The NNLO cross section is also shown in Fig. 4 (red star points) in order to put in evidence the size of the N<sup>3</sup>LO corrections respect to the precedent perturbative order. The total cross sections shown in Fig. 4 are explicitly reported in Table 2.

## 4 The rapidity distribution of the Higgs boson

In this section we make use of the  $C_{N3}$  coefficient (computed in Sec. 3.1) producing differential predictions at N<sup>3</sup>LO. In particular we present completely differential results for the rapidity of the Higgs boson. In Sec. 4.1 we estimate at NNLO the uncertainties introduced in the rapidity distribution, by the procedure proposed in Eq. (41). In Sec. 4.2 we present the rapidity distribution at N<sup>3</sup>LO with the corresponding estimation of the uncertainties associated to the variation of the  $q_T^{cut}$  and  $C_{N3}$  parameters.

n	$[\tilde{\mu}_R, \tilde{\mu}_F] \times M_H$	$C_{N3} (q_T^{\text{cut}} = 1 \text{ GeV})$	$C_{N3} (q_T^{\text{cut}} = 2 \text{ GeV})$	$C_{N3} (q_T^{\text{cut}} = 3 \text{ GeV})$
(1)	$[1/2, 1/2]$	<b><math>-943 \pm 222</math></b>	$-967 \pm 179$	$-988 \pm 164$
(2)	$[1, 1]$	<b><math>-971 \pm 207</math></b>	$-965 \pm 168$	$-989 \pm 151$
(3)	$[1/4, 1/4]$	<b><math>-883 \pm 243</math></b>	$-866 \pm 198$	$-850 \pm 162$
(4)	$[1/2, 1]$	$-986 \pm 222$	$-1021 \pm 179$	$-1033 \pm 179$
(5)	$[1, 1/2]$	$-990 \pm 206$	$-976 \pm 167$	$-968 \pm 158$
(6)	$[1/2, 1/4]$	$-985 \pm 221$	$-978 \pm 181$	$-923 \pm 152$
(7)	$[1/4, 1/2]$	$-977 \pm 243$	$-859 \pm 199$	$-883 \pm 179$

Table 1: Predicted values of the  $C_{N3}$  coefficients as a function of the  $q_T^{\text{cut}}$  as shown in Fig. 3 for each scale choice (second column). In bold typeface the  $C_{N3}$  coefficients (for the case  $q_T^{\text{cut}} = 1 \text{ GeV}$ ) which are used to compute the averaged value  $C_{N3} = -932 \pm 222$  shown in Figs. 2 and 3, with the central red line and the corresponding red band. The uncertainty for each one of the  $C_{N3}$  coefficients is calculated with the customary propagations of the uncertainties. The first column is used to label each particular scale choice and used in Fig. 3.

$\sigma$ (pb)	Exact	$q_T$ subtraction ( $q_T^{\text{cut}} = 1 \text{ GeV}$ )	$q_T$ subtraction ( $q_T^{\text{cut}} = 2 \text{ GeV}$ )	$q_T$ subtraction ( $q_T^{\text{cut}} = 3 \text{ GeV}$ )	$q_T$ subtraction ( $C_{N3} = 0$ )
N <sup>3</sup> LO [ $\mu = M_H/2$ ]	44.97	$44.98 \pm 0.21$	$45.00 \pm 0.17$	$45.02 \pm 0.15$	$45.86 \pm 0.21$
N <sup>3</sup> LO [ $\mu = M_H$ ]	43.50	$43.52 \pm 0.12$	$43.52 \pm 0.10$	$43.53 \pm 0.09$	$44.08 \pm 0.12$
N <sup>3</sup> LO [ $\mu = M_H/4$ ]	45.06	$44.98 \pm 0.38$	$44.96 \pm 0.31$	$44.93 \pm 0.28$	$46.44 \pm 0.38$
NNLO [ $\mu = M_H/2$ ]	43.47	$43.58 \pm 0.11$	$43.58 \pm 0.11$	$43.58 \pm 0.11$	$43.58 \pm 0.11$
NNLO [ $\mu = M_H$ ]	39.64	$39.69 \pm 0.04$	$39.69 \pm 0.04$	$39.69 \pm 0.04$	$39.69 \pm 0.04$
NNLO [ $\mu = M_H/4$ ]	47.33	$47.50 \pm 0.18$	$47.50 \pm 0.18$	$47.50 \pm 0.18$	$47.50 \pm 0.18$

Table 2: The total cross section for Higgs boson production at the LHC ( $\sqrt{s} = 13 \text{ TeV}$ ). Results for NNLO and N<sup>3</sup>LO cross sections for three different scales  $\mu = M_H/2$  (central scale),  $\mu = M_H$  and  $\mu = M_H/4$ . The column “Exact” contains the results of Ref. [25] computed with the numerical code of Ref. [26]. The results with the  $q_T$  subtraction method are obtained using three different values of  $q_T^{\text{cut}}$  (1, 2 and 3 GeV), and their uncertainties are calculated with the customary propagation of statistical errors. The last column shows the total cross sections obtained with the  $q_T$  subtraction method and using  $C_{N3} = 0$  at N<sup>3</sup>LO. The values of the total cross sections reported in this Table are shown in Fig. 4. The NNLO cross sections computed with the  $q_T$  subtraction method are obtained using  $q_T^{\text{cut}} = 1 \text{ GeV}$ , i.e., the variation of this parameter in the N<sup>3</sup>LO cross section is considered only at N<sup>3</sup>LO exclusively.

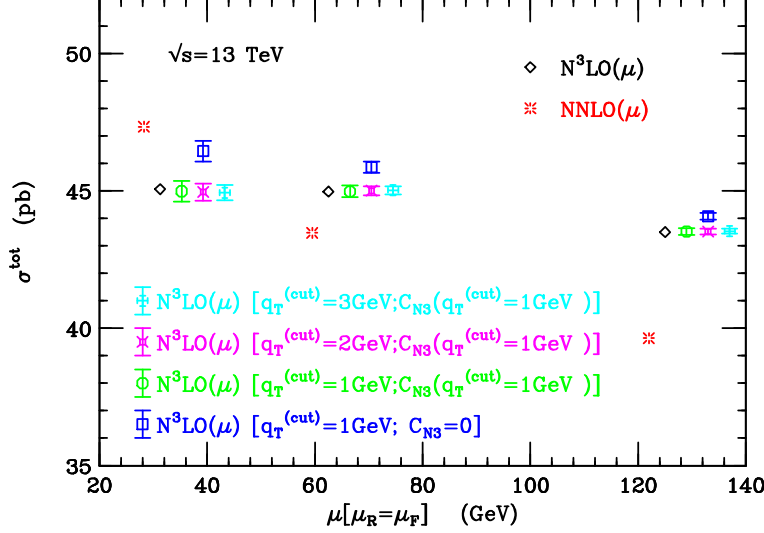


Figure 4: Total Higgs boson cross section at  $N^3LO$ , as predicted by the  $q_T$  subtraction formalism, compared with the analytical Higgs boson total cross section at  $N^3LO$  of Ref. [25] (black diamonds). In green points we present the  $q_T$  subtraction prediction for  $q_T^{cut}=1$  GeV. In magenta points we consider the  $N^3LO$  cross section using  $q_T^{cut}=2$  GeV, and in cyan the corresponding cross section using  $q_T^{cut}=3$  GeV. Whereas the  $q_T^{cut}$  is changed (from 1 to 3 GeV) the coefficient  $C_{N3}$  is always considered the same (as calculated in Fig. 2 for  $q_T^{cut}=1$  GeV). The  $q_T$  subtraction prediction at  $N^3LO$  with the  $C_{N3}$  numerical coefficient fixed to zero (using  $q_T^{cut}=1$  GeV) is shown with blue squared points. The NNLO analytical Higgs boson cross section is presented in pink star points. All the cross sections are shown for three different scales:  $\mu \equiv \mu_R = \mu_F = \{1/4, 1/2, 1\}M_H$ . The uncertainty bars in the  $q_T$  subtraction predictions are calculated with the customary propagation of statistical uncertainties.

#### 4.1 The NNLO rapidity distribution

The aim of the present section is quantify the uncertainty in the approximation proposed in Eq. (41). Since at NNLO all the ingredients of the  $q_T$  subtraction formalism are known, it is possible to evaluate the deviation from the exact result. For the present quantitative exercise we take as known the collinear functions  $C_{ga}^{(1)}$  and the hard-virtual factor  $H_g^{H(1)}$  in Eq. (38). The collinear functions  $C_{ga}^{(2)}$  and the first order helicity-flip functions  $G_{ga}^{(1)}$  are regarded as unknown. The hard-virtual factor  $H_g^{H(2)}$  is divided in two contributions as in Eq. (40)

$$\tilde{H}_g^{H(2)} \equiv H_g^{H(2)} - [H_g^{H(2)}]_{(\delta_{(1)}^{q_T})}, \quad (42)$$

where  $[H_g^{H(2)}]_{(\delta_{(1)}^{q_T})}$  is considered as unknown for the present NNLO study. The so called *unknown functions* (for this exercise) which depend on the variable  $z$  in Eq. (38) are approximated with a single numerical coefficient  $C_N$  proportional to  $\delta(1-z)$

$$C_N \delta_{ga} \delta_{gb} \delta(1-z) \leftarrow \delta_{ga} \delta_{gb} \delta(1-z) [H_g^{H(2)}]_{(\delta_{(1)}^{q_T})} + \delta_{ga} C_{gb}^{(2)}(z) + \delta_{gb} C_{ga}^{(2)}(z) + \left( G_{ga}^{(1)} \otimes G_{gb}^{(1)} \right)(z). \quad (43)$$



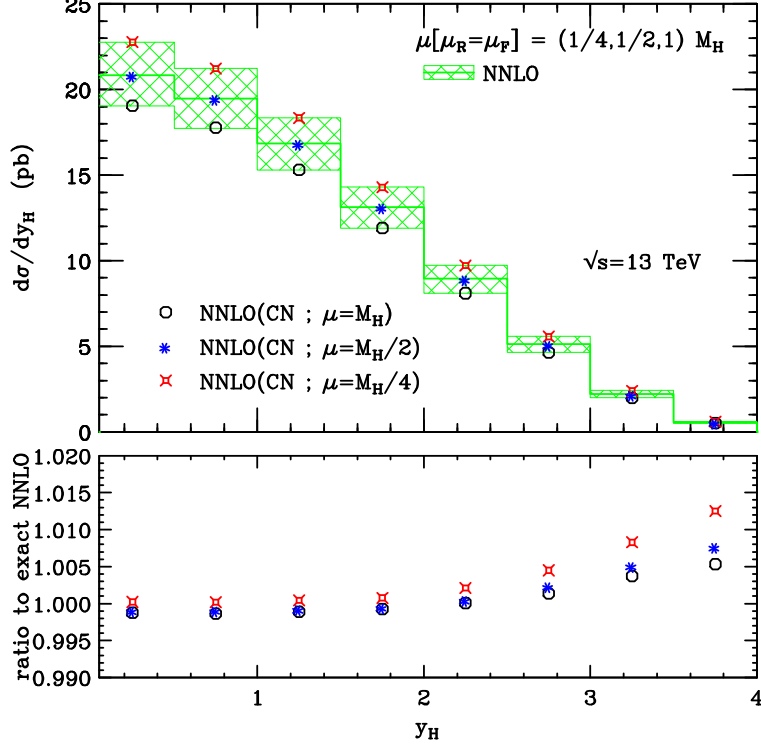


Figure 5: *Rapidity distribution at NNLO as predicted by the  $q_T$  subtraction formalism (solid green band) compared with the prediction using the  $C_N$  numerical coefficient (red, blue and black points). In the lower panel we show the ratio to the exact NNLO result. For this particular example at NNLO, we employ the three points scale variation:  $\mu = \mu_R = \mu_F = \{M_H/4, M_H/2, M_H\}$ .*

In Fig. 5 we show the rapidity distribution of the Higgs boson at NNLO computed with the exact  $q_T$  subtraction (green band) and the NNLO prediction using the  $C_N$  coefficient (red, blue and black points). For this particular example at NNLO, we employ the three-point scale variation:  $\mu = \mu_R = \mu_F = \{M_H/4, M_H/2, M_H\}$ .

In the lower panel of Fig. 5 we show the ratio to the exact NNLO result, i.e we present the ratio for each scale. As expected, the approximation presents its best behaviour at central rapidity and for  $|y_H| \leq 3.5$  it is at the *sub percent* level.

The numerical implementation of the  $q_T$  subtraction method (more precisely Eq. (35) at NNLO) requires the implementation of a lower technical cut ( $q_T^{\text{cut}}$ ) in the integral performed over the transverse momentum of the finite contribution in Eq. (32). We postpone the discussion of the choice of  $q_T^{\text{cut}}$  to Section 4.2. The computation of the NNLO Higgs boson cross section and differential distributions do not represent a technical challenge, and the  $q_T^{\text{cut}}$  can be considered as low as the computation demands. We performed variations of the  $q_T^{\text{cut}}$  between 0.1 GeV and 3 GeV, and the NNLO cross sections (and differential distributions) present deviations within a 0.5% level of accuracy (the largest deviation 0.5% is always manifested for the scale choice  $\mu = M_H/4$ ).

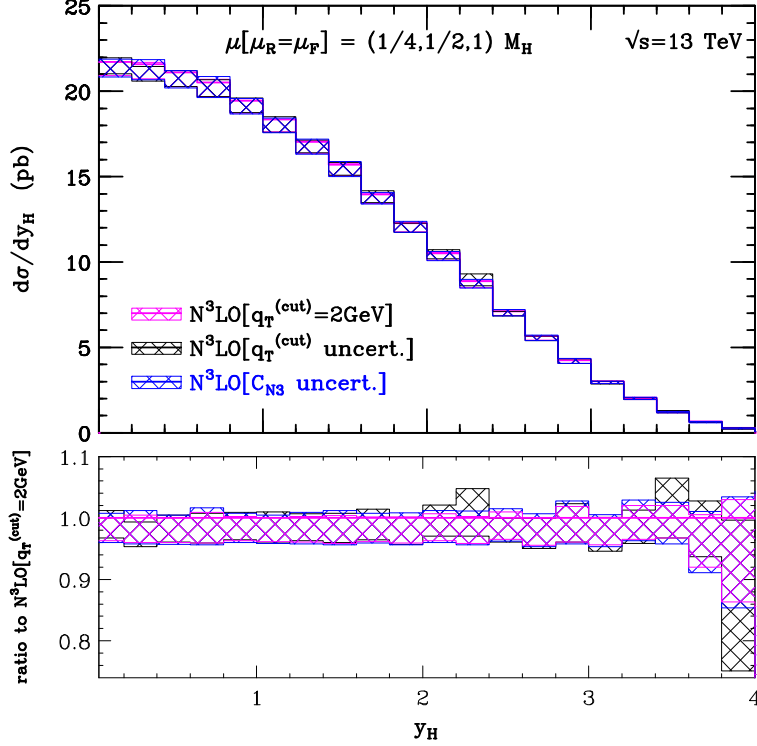


Figure 6: Rapidity distribution of the Higgs boson as predicted by the  $q_T$  subtraction formalism at  $N^3\text{LO}$ . The bands are the result of the variation of the scales at seven-point as detailed in Table 2. The magenta band constitutes our prediction using  $q_T^{\text{cut}} = 2 \text{ GeV}$ . The black band is obtained as the envelope between the prediction at  $q_T^{\text{cut}} = 1 \text{ GeV}$  and  $2\text{GeV}$  and the blue band is computed varying the  $C_{N3}$  coefficient for each one of the seven scales accordingly the calculated uncertainty for this third order coefficient as described in the text.

## 4.2 The rapidity of the Higgs boson at $N^3\text{LO}$

We start the presentation of our first results for the rapidity distribution of the Higgs boson at  $N^3\text{LO}$ .

In Fig. (6) we show the rapidity distribution at  $N^3\text{LO}$  obtained with the  $q_T$  subtraction method using the  $C_{N3}$  coefficient calculated in Sec. 3.1 ( $C_{N3} = -932 \pm 222$ ). The magenta band in Fig. (6) is computed using  $q_T^{\text{cut}} = 2 \text{ GeV}$  and performing the seven-point scale variation specified in Table 2. The black band is calculated as the envelope of the rapidity bands for two different values of  $q_T^{\text{cut}}$  (1 GeV and 2GeV). Therefore, the black band in Fig. (6) can be taken as the estimation of the uncertainty due to the implementation of different  $q_T^{\text{cut}}$  parameters at  $N^3\text{LO}$  exclusively. The NNLO prediction is always computed with  $q_T^{\text{cut}} = 1 \text{ GeV}$ . Notice the following consideration: in Fig. (4) (and also in Table 2) the total cross section (for the three central scales) is rather stable as a function of the  $q_T^{\text{cut}}$ . The variations of the  $N^3\text{LO}$  cross sections are at the *per mille* level of accuracy if we consider  $q_T^{\text{cut}} = 2 \pm 1 \text{ GeV}$ , which is far better than the associated statistical uncertainty (see Table 2). The estimation of the uncertainty due to the  $q_T^{\text{cut}}$  variation performed in Fig. (6) (which is differential in the rapidity of the Higgs boson) confirms the precedent considerations: while the rapidity is almost insensitive to the change in the  $q_T^{\text{cut}}$  parameter where the bulk of the cross section takes place ( $|y_H| \leq 3.6$ ), at large rapidities, where

the contribution to the total cross section is less than the 0.5%, we found the largest deviations.

Finally, we consider the uncertainty due to the statistical errors of the  $C_{N3}$  coefficient. The blue band in Fig. (6) is obtained as the envelope of the seven scales variation at  $q_T^{\text{cut}} = 2$  GeV but considering for each scale two different  $C_{N3}$  values: more clearly, the two extremal  $C_{N3}$  coefficients corresponding to its maximum and minimum statistical deviations  $C_{N3} = (-1154, -710)$ . The net effect of this  $C_{N3}$  variation result in an overall enlargement of the customary magenta band at  $q_T^{\text{cut}} = 2$  GeV. Our final estimation of the uncertainties in the rapidity of the Higgs boson at N<sup>3</sup>LO is computed as the envelope of the three bands presented in Fig. (6).

## 5 Final results

In this section we present our best estimation for the Higgs boson rapidity at the LHC, applying the N<sup>3</sup>LO  $q_T$  subtraction method presented in Sec. 2. The setup of the calculation was stated in Sec. 3.1.

In Fig. 7 we show the rapidity distribution of the Higgs boson at LO (dashed black band), NLO (blue solid band), NNLO (green solid band) and N<sup>3</sup>LO (magenta solid band). The N<sup>3</sup>LO band is computed taking into account the uncertainties due to  $q_T^{\text{cut}}$  and  $C_{N3}$  as explained in Sec. 4.2.

The central scale ( $\mu = M_H/2$ ) is shown with a solid line while the variation of the scales by a factor  $\{1/2, 2\}$  produce the seven-point scale band. It is interesting to notice that from LO to NNLO, the scale  $\mu = M_H/2$  is always at the center of the corresponding scale variation band in Fig. 7. At N<sup>3</sup>LO the central scale  $\mu = M_H/2$  (magenta solid line) almost coincides with the limit of the upper band. The precedent fact is the differential manifestation of what was shown in Fig. 4 for the total cross section: for  $\mu = M_H/4$  and  $\mu = M_H/2$  the N<sup>3</sup>LO cross sections are in accord at the 0.2% level, noticing that the scale  $\mu = M_H/4$  is at the top of the scale variation band for the whole rapidity range. The Figs. 4 and 7 show the reduction in the size of the variation of the scales at N<sup>3</sup>LO, in the total cross section and in differential distributions, respectively.

The impact of the N<sup>3</sup>LO corrections on the NNLO result is almost independent of the rapidity  $y_H$  in the entire rapidity range  $|y_H| \leq 4$ . The total cross section (for the central scale) increases by about 3.4% when going from NNLO to N<sup>3</sup>LO.

## 6 Conclusions

**Acknowledgements.**

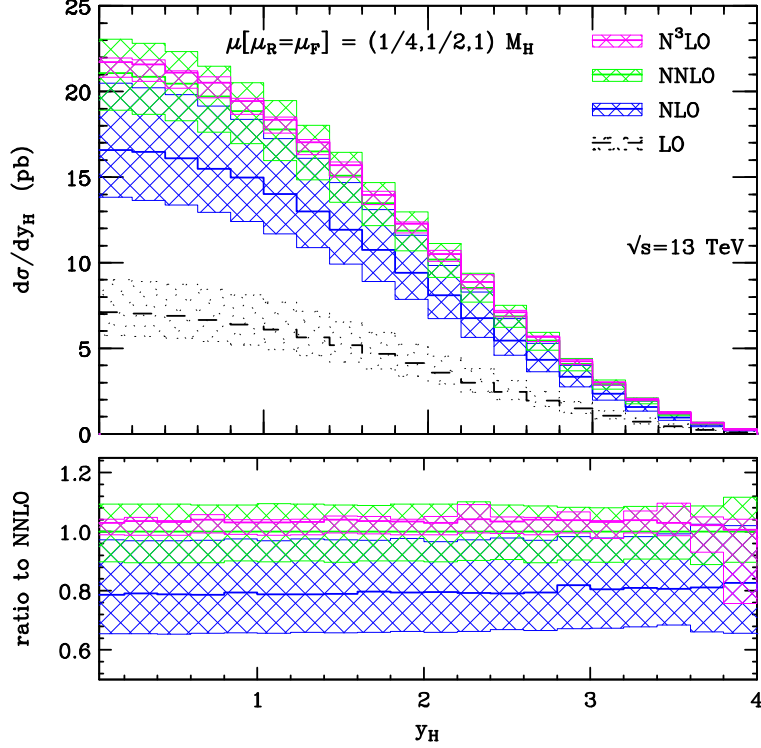


Figure 7: Rapidity distribution of the Higgs boson as predicted by the  $q_T$  subtraction formalism up to  $N^3\text{LO}$ . The seven-point scale variation bands of the LO, NLO, NNLO and  $N^3\text{LO}(C_{N3})$  results are as follows: LO (black dashed), NLO (blue solid), NNLO (green solid) and  $N^3\text{LO}(C_{N3})$  (magenta solid). The central scale ( $\mu = M_H/2$ ) at each perturbative order, is shown with solid lines respecting the colour of the corresponding perturbative order. In the lower panel, the ratio to the NNLO prediction is shown. While the bands for the predictions at LO, NLO and NNLO are computed with the seven scales as detailed in the text, the  $N^3\text{LO}(C_{N3})$  band is obtained after considering also the uncertainties due to the variation of the  $q_T^{\text{cut}}$  and the  $C_{N3}$  coefficient.

## 7 Appendix: Convolutions at $N^3\text{LO}$

The numerical implementation of Eq. (7) requires the computation of several convolutions between splitting functions, collinear and helicity-flip functions. In principle, taking the  $N$ -moments of the functions involved in the calculation, one can avoid the use of convolutions, since in  $N$ -space they are simply products. However the numerical implementation of Eq. (7) on the Monte Carlo code HN3LO was carried out in the  $z$ -space (e.g as in the codes HNNLO [1], DYNNLO [27], 2 $\gamma$ NNLO [28], etc), and therefore the new third order convolutions have to be calculated as well.

The convolutions in Eqs. (38), (39), (41) and (43) between two functions ( $f(z)$  and  $g(z)$ ) of the the variable  $z$  are defined through the following integral

$$(f \otimes g)(z) \equiv \int_z^1 \frac{dy}{y} f\left(\frac{z}{y}\right) g(y). \quad (44)$$

In the case of processes initiated by gluon fusion, the complete list of third order convolutions to be calculated can be found in Table 3. All the remaining convolutions in Eq. (7) at  $N^3\text{LO}$

(i)	$\gamma_{ga_1}^{(1)} \otimes \gamma_{a_1 a_2}^{(1)} \otimes \gamma_{a_2 g}^{(1)}$	(ii)	$\gamma_{ga_1}^{(1)} \otimes \gamma_{a_1 a_2}^{(1)} \otimes \gamma_{a_2 q}^{(1)}$
(iii)	$\gamma_{ga}^{(1)} \otimes \gamma_{ag}^{(2)}$	(iv)	$\gamma_{ga}^{(1)} \otimes \gamma_{aq}^{(2)}$
(v)	$\gamma_{ga}^{(2)} \otimes \gamma_{ag}^{(1)}$	(vi)	$\gamma_{ga}^{(2)} \otimes \gamma_{aq}^{(1)}$
(vii)	$C_{ga}^{(1)} \otimes \gamma_{ag}^{(2)}$	(viii)	$C_{ga}^{(1)} \otimes \gamma_{aq}^{(2)}$
(ix)	$C_{ga}^{(2)} \otimes \gamma_{ag}^{(1)}$	(x)	$C_{ga}^{(2)} \otimes \gamma_{aq}^{(1)}$
(xi)	$G_{ga}^{(1)} \otimes \gamma_{ag}^{(1)}$	(xii)	$G_{ga}^{(1)} \otimes \gamma_{aq}^{(1)}$

Table 3: *Convolutions appearing at the  $N^3LO$  exclusively between the collinear  $C_{a_1 a_2}^{(n)}$ , the helicity-flip  $G_{a_1 a_2}^{(n)}$  and the splitting functions  $\gamma_{a_1 a_2}^{(n)}$  ( $n = 1, 2$ ). The repeated subindices  $a, a_1$  and  $a_2$  imply a sum over the parton flavors  $q, \bar{q}, g$ . The first and last subindices denote the partonic channel in which they are contributing, i.e the convolutions in the first column are used in the  $gg$  partonic channel whereas the second (and last) column is for the  $qg$  and  $gq$  partonic channels.*

already contributed to the previous orders and they are regarded as known. The symbol  $\gamma_{ab}^{(n)}$  in Table 3 denotes the usual splitting functions of  $n$ -order and they contribute to Eq. (7) since the PDFs have to be evolved from the scale  $b_0^2/b^2$  to the customary factorization scale  $\mu_F$ . The first three rows in Eq. (3) were calculated in Ref. [30] and cross checked with a dedicated computation for the results presented in this paper. The **Mathematica** public code **MT** [29] used to calculate the necessary convolutions (i)–(vi) in Ref. [30] is allowed to provide the resulting convolutions in terms of *Harmonic Poly-Logarithms* (HPLs) [32] exploiting the **Mathematica** package **HPL** [31]. The remaining convolutions in Eqs. (vii)–(xii) of Table 3 were computed in particular for this work. The **MT** [29] package is not able to solve all the convolutions of weight 3 and 4 that are needed in (vii)–(xii). For instance the **MT** package can not handle convolutions in which their result has to be expressed in terms of multiple poly-logarithms (or *Goncharov Poly-Logarithms* GPLs) [33, 34] as it is the case when the collinear functions  $C_{gj}^{(2)}$  are involved. Owing to the precedent reasons we computed the convolutions (vii)–(xii) with the code **Convo** which is able to provide results in terms of GPLs and also can handle with terms separately divergent but finite after addition.

The multiple poly-logarithms can be defined recursively, for  $n \geq 0$ , via the iterated integral [33, 34]

$$G(a_1, \dots, a_n; z) = \int_0^z \frac{dt}{t - a_1} G(a_2, \dots, a_n; t), \quad (45)$$

with  $G(z) = G(; z) = 1$  (an exception being when  $z = 0$  in which case we put  $G(0) = 0$ ) and with  $a_i \in \mathbb{C}$  are chosen constants and  $z$  is a complex variable. Nevertheless, for the convolutions in Table 3 the following conditions verify: the variable  $z \in \mathbb{R}$  and the weights  $a_1, \dots, a_n \in \mathbb{R}$ .

Among the required convolutions in Table 3 we list some of them which appear as building

(a)	$G(\frac{z}{1+z}, 0, 0, 1; \frac{1}{2})$	(b)	$G(1, 0, 0, -z; z)$	(c)	$G(0, 1, 0, -1; z)$
(d)	$G(0, 1, 0, z; 1)$	(e)	$G(0, 1, z, 0; 1)$	(f)	$G(0, z, 1, 0; 1)$
(g)	$G(-z, 0, z, 0; 1)$	(h)	$G(0, 1, 0, -z; z)$	(i)	$G(0, 1, -z, -z; z)$
(j)	$G(-z, 1, 0, 0; 1)$	(k)	$G(-z, 1, 0, 0; z)$	(l)	$G(-z, 0, 0, z; 1)$

Table 4: *Basis for the GPLs used in the numerical implementation of the convolutions listed in Table 3. The basis is not unique, however its length is enough for a straightforward numerical implementation in the Monte Carlo generator.*

blocks in the course of the computation of Eqs. (vii)–(xii) in Table 3,

$$\left\{ D_0[1-y]; \frac{1}{y}; 1; y; y^2 \right\} \otimes \left( \frac{f(y)}{1+y} \right) , \quad (46)$$

$$f(y) = \left\{ \text{Li}_3 \left( \frac{1}{1+y} \right); \text{Li}_3(\pm y); \text{Li}_2(\pm y); \text{Li}_2(1-y); \text{Li}_2(\pm y) \ln(y); \right. \\ \left. \ln^2(1+y) \ln(y); \ln(1+y) \ln^2(y) \right\} , \quad (47)$$

where the customary *plus* distribution  $D_0[1-z]$  is defined as usual

$$\int_0^1 dz f(z) D_0[1-z] = \int_0^1 dz \frac{f(z)}{(1-z)_+} = \int_0^1 \frac{dz}{1-z} (f(z) - f(1)) . \quad (48)$$

After performing all the convolutions listed in Table 3, their final expressions (each one of the convolutions) are finite in the domain  $z \in (0, 1)$ . Even more, convolutions when evaluated in the domain  $z \in (0, 1)$  produce results belonging to  $\mathbb{R}$ . It is possible to write the expressions in Table 3 (after simplifying) in function of twelve GPLs that are not reducible to *classic* functions or can not be combined (e.g through the *shuffle* algebra) with other GPLs in order to produce simpler results. Here the adjective *classic* is used to mean functions that do not require the numerical implementation of specific packages to handle GPLs or HPLs, for instance:  $\text{Li}_i(z)$  ( $0 \leq i \leq 4$ ) and polynomials of the variable ( $0 \leq z \leq 1$ ).

The list of the irreducible GPLs is presented in Table 4. All the other GPLs appearing in the resulting convolutions of Table 3 can be related to the set of Table 4 using the results of Refs. [36, 31, 35] and performing the customary *shuffle* algebra. The numerical implementation of the GPLs in Table 4 was made using the package **GiNaC** [37]. The basis of GPLs in Table 4 is not unique, but its present form is enough for a reasonable numerical evaluation *event-by-event*.

As an example of a third order convolution we can perform the following integral

$$\begin{aligned}
\left( \frac{\text{Li}_3(y)}{1+y} \otimes \text{D}_0[1-y] \right) (z) &= \int_z^1 \frac{dy}{y+z} \text{Li}_3\left(\frac{z}{y}\right) \frac{1}{(1-y)_+} = \frac{1}{1+z} \left( -\zeta_3 G(0; z) + \frac{i\pi^3}{6} G(0; z) \right. \\
&+ \frac{\pi^2}{3} G(-z; 1) G(0; z) - i\pi G(-z, 0; 1) G(0; z) - G(-z, 0, 0; 1) G(0; z) + \frac{i\pi\zeta_3}{4} + \frac{\pi^2}{3} G(0, 1; z) \\
&+ i\pi G(-z; 1) G(0, 0; z) - \frac{\pi^2}{6} G(0, 0; z) - G(-z; 1) G(0, 0, 0; z) + i\pi G(0, 0, 1; z) \\
&+ G(0, 0; z) G(-z, 0; 1) - \frac{\pi^2}{3} G(-z, 0; 1) + i\pi G(-z, 0, 0; 1) - G(0, 0, 0, 1; z) \\
&- G(0, 0, 1, z; 1) - G(0, 0, z, 1; 1) - G(0, 1, 0, z; 1) - G(1, 0, 0, z; z) + G(-z, 0, 0, 0; 1) \\
&\left. - G(-z, 0, 0, z; 1) + G(-z, 0, 0, z; z) + \frac{19\pi^4}{720} \right) . \tag{49}
\end{aligned}$$

Notice that with the rescaling property of the GPLs

$$G(k(a_1 \dots a_n); kx) = G(a_1 \dots a_n; x) \quad \text{with } (a_n \neq 0) \text{ and } (k \in \mathbb{C}^*) , \tag{50}$$

it is possible to write some GPLs in Eq. (49) as HPLs. After performing all the convolutions in Table 3 and applying the precedent properties (satisfied by the GPLs), it is possible to arrive to the set detailed in Table 4. The rescaling property of Eq. (50) can be used also to relate the GPL in Eq. (l) in Table 4 with the one in Eq. (c) of the same Table (*modulo* functions of the type  $\text{Li}_i(z)$  ( $0 \leq i \leq 4$ ) and polynomials in the variable ( $0 \leq z \leq 1$ )) after some algebra. However this procedure leads to the numerical evaluation of Eq. (c) in Table 4 in a different argument ( $1/z$ ), which from a purely numerical point of view, does not represent any improvement. Therefore the GPL basis in Table 4 has to be taken as irreducible in a numerical sense, since it represents the smallest numerical cost *event-by-event*.

## References

- [1] S. Catani and M. Grazzini, Phys. Rev. Lett. **98** (2007) 222002 [hep-ph/0703012].
- [2] G. Bozzi, S. Catani, D. de Florian and M. Grazzini, Nucl. Phys. B **737** (2006) 73 [hep-ph/0508068].
- [3] G. Bozzi, S. Catani, D. de Florian and M. Grazzini, Phys. Lett. B **564** (2003) 65.
- [4] A. Gehrmann-De Ridder, T. Gehrmann and E. W. N. Glover, JHEP **0509** (2005) 056 [hep-ph/0505111]; A. Gehrmann-De Ridder, T. Gehrmann and E. W. N. Glover, Phys. Lett. B **612** (2005) 49 [hep-ph/0502110]; A. Gehrmann-De Ridder, T. Gehrmann and E. W. N. Glover, Phys. Lett. B **612** (2005) 36 [hep-ph/0501291]; A. Daleo, T. Gehrmann and D. Maitre, JHEP **0704** (2007) 016 [hep-ph/0612257]; A. Daleo, A. Gehrmann-De Ridder, T. Gehrmann and G. Luisoni, JHEP **1001** (2010) 118 [arXiv:0912.0374 [hep-ph]]; R. Boughezal, A. Gehrmann-De Ridder and M. Ritzmann, JHEP **1102** (2011) 098 [arXiv:1011.6631 [hep-ph]]; T. Gehrmann and P. F. Monni, JHEP **1112** (2011) 049 [arXiv:1107.4037 [hep-ph]]; A. Gehrmann-De Ridder, T. Gehrmann and M. Ritzmann, JHEP **1210** (2012) 047 [arXiv:1207.5779 [hep-ph]]; J. Currie, E. W. N. Glover and S. Wells, JHEP **1304** (2013) 066 [arXiv:1301.4693 [hep-ph]].

- [5] Y. L. Dokshitzer, D. Diakonov and S. I. Troian, Phys. Lett. B **79** (1978) 269, Phys. Rep. **58** (1980) 269; G. Parisi and R. Petronzio, Nucl. Phys. B **154** (1979) 427. G. Curci, M. Greco and Y. Srivastava, Nucl. Phys. B **159** (1979) 451; J. C. Collins and D. E. Soper, Nucl. Phys. B **193** (1981) 381 [Erratum-ibid. B **213** (1983) 545], Nucl. Phys. B **197** (1982) 446; J. Kodaira and L. Trentadue, Phys. Lett. B **112** (1982) 66, report SLAC-PUB-2934 (1982), Phys. Lett. B **123** (1983) 335; J. C. Collins, D. E. Soper and G. Sterman, Nucl. Phys. B **250** (1985) 199; S. Catani, E. D’Emilio and L. Trentadue, Phys. Lett. B **211** (1988) 335; D. de Florian and M. Grazzini, Phys. Rev. Lett. **85** (2000) 4678 [arXiv:hep-ph/0008152];  
S. Catani, D. de Florian and M. Grazzini, Nucl. Phys. B **596** (2001) 299 [arXiv:hep-ph/0008184].
- [6] S. Catani and M. Grazzini, Nucl. Phys. B **845** (2011) 297 [arXiv:1011.3918 [hep-ph]].
- [7] S. Catani, L. Cieri, D. de Florian, G. Ferrera and M. Grazzini, Nucl. Phys. B **881** (2014) 414 doi:10.1016/j.nuclphysb.2014.02.011 [arXiv:1311.1654 [hep-ph]].
- [8] S. Catani, D. de Florian and M. Grazzini, Nucl. Phys. B **596** (2001) 299 [arXiv:hep-ph/0008184].
- [9] O. V. Tarasov, A. A. Vladimirov and A. Y. Zharkov, Phys. Lett. **93B** (1980) 429. doi:10.1016/0370-2693(80)90358-5
- [10] S. A. Larin and J. A. M. Vermaseren, Phys. Lett. B **303** (1993) 334 doi:10.1016/0370-2693(93)91441-O [hep-ph/9302208].
- [11] D. de Florian and M. Grazzini, Nucl. Phys. B **616** (2001) 247 [arXiv:hep-ph/0108273].
- [12] S. Catani and M. Grazzini, Eur. Phys. J. C **72** (2012) 2013 [Erratum-ibid. C **72** (2012) 2132] [arXiv:1106.4652 [hep-ph]].
- [13] S. Catani, L. Cieri, D. de Florian, G. Ferrera and M. Grazzini, Eur. Phys. J. C **72** (2012) 2195 [arXiv:1209.0158 [hep-ph]].
- [14] G. Curci, W. Furmanski and R. Petronzio, Nucl. Phys. B **175** (1980) 27.
- [15] W. Furmanski and R. Petronzio, Phys. Lett. B **97** (1980) 437.
- [16] R. V. Harlander and K. J. Ozeren, Phys. Lett. B **679** (2009) 467 [arXiv:0907.2997 [hep-ph]];
- [17] M. Spira, A. Djouadi, D. Graudenz and P. M. Zerwas, Nucl. Phys. B **453** (1995) 17 [hep-ph/9504378].
- [18] Y. Li and H. X. Zhu, Phys. Rev. Lett. **118** (2017) no.2, 022004 doi:10.1103/PhysRevLett.118.022004 [arXiv:1604.01404 [hep-ph]].
- [19] A. A. Vladimirov, Phys. Rev. Lett. **118** (2017) no.6, 062001 doi:10.1103/PhysRevLett.118.062001 [arXiv:1610.05791 [hep-ph]].
- [20] S. Catani, L. Cieri, D. de Florian, G. Ferrera and M. Grazzini, Nucl. Phys. B **888** (2014) 75 doi:10.1016/j.nuclphysb.2014.09.012 [arXiv:1405.4827 [hep-ph]].
- [21] T. Becher, M. Neubert, Eur. Phys. J. **C71** (2011) 1665 [arXiv:1007.4005 [hep-ph]].



- [22] R. D. Ball *et al.* [NNPDF Collaboration], JHEP **1504** (2015) 040 [arXiv:1410.8849].
- [23] X. Chen, J. Cruz-Martinez, T. Gehrmann, E. W. N. Glover and M. Jaquier, JHEP **1610** (2016) 066 doi:10.1007/JHEP10(2016)066 [arXiv:1607.08817 [hep-ph]].
- [24] A. Buckley, J. Ferrando, S. Lloyd, K. Nordström, B. Page, M. Rfenacht, M. Schnherr and G. Watt, Eur. Phys. J. C **75** (2015) 132 doi:10.1140/epjc/s10052-015-3318-8 [arXiv:1412.7420 [hep-ph]].
- [25] B. Mistlberger, arXiv:1802.00833 [hep-ph].
- [26] F. Dulat, A. Lazopoulos and B. Mistlberger, arXiv:1802.00827 [hep-ph].
- [27] S. Catani, L. Cieri, G. Ferrera, D. de Florian and M. Grazzini, Phys. Rev. Lett. **103** (2009) 082001 doi:10.1103/PhysRevLett.103.082001 [arXiv:0903.2120 [hep-ph]].
- [28] S. Catani, L. Cieri, D. de Florian, G. Ferrera and M. Grazzini, Phys. Rev. Lett. **108** (2012) 072001 Erratum: [Phys. Rev. Lett. **117** (2016) no.8, 089901] doi:10.1103/PhysRevLett.108.072001, 10.1103/PhysRevLett.117.089901 [arXiv:1110.2375 [hep-ph]].
- [29] M. Hschele, J. Hoff, A. Pak, M. Steinhauser and T. Ueda, Comput. Phys. Commun. **185** (2014) 528 doi:10.1016/j.cpc.2013.10.007 [arXiv:1307.6925 [hep-ph]].
- [30] M. Hschele, J. Hoff, A. Pak, M. Steinhauser and T. Ueda, Phys. Lett. B **721** (2013) 244 doi:10.1016/j.physletb.2013.03.003 [arXiv:1211.6559 [hep-ph]].
- [31] D. Maitre, Comput. Phys. Commun. **174** (2006) 222 doi:10.1016/j.cpc.2005.10.008 [hep-ph/0507152].
- [32] E. Remiddi and J. A. M. Vermaseren, Int. J. Mod. Phys. A **15** (2000) 725 doi:10.1142/S0217751X00000367 [hep-ph/9905237].
- [33] A. B. Goncharov, Math. Res. Lett. **5** (1998) 497 doi:10.4310/MRL.1998.v5.n4.a7 [arXiv:1105.2076 [math.AG]].
- [34] A. B. Goncharov, math/0103059 [math.AG].
- [35] C. Duhr, H. Gangl and J. R. Rhodes, JHEP **1210** (2012) 075 doi:10.1007/JHEP10(2012)075 [arXiv:1110.0458 [math-ph]].
- [36] H. Frellesvig, D. Tommasini and C. Wever, JHEP **1603** (2016) 189 doi:10.1007/JHEP03(2016)189 [arXiv:1601.02649 [hep-ph]].
- [37] C. W. Bauer, A. Frink and R. Kreckel, J. Symb. Comput. **33** (2000) 1 [cs/0004015 [cs-sc]].